Med Biol Eng Comput (2014) 52:797–811
DOI 10.1007/s11517-014-1181-7

ORIGINAL ARTICLE

Evaluation of the hemodynamics in straight 6-mm and tapered 6- to 8-mm grafts as upper arm hemodialysis vascular access

M. Sarmast · H. Niroomand-Oscuii · F. Ghalichi · E. Samiei

Received: 10 May 2013 / Accepted: 25 July 2014 / Published online: 12 August 2014
© International Federation for Medical and Biological Engineering 2014

Abstract The present study is intended to investigate and compare the hemodynamics in two different sizes of hemodialysis arteriovenous grafts for upper arm hemodialysis vascular access: 8-mm tapered to 6-mm at the arterial side and straight 6 mm. A computational simulation approach is presented for this study, which is validated against the available experimental and numerical pressure measurements in the literature. The imposed boundary conditions at the arterial inlet and venous outlet boundaries of the models are physiological velocity and pressure waveforms, respectively. Blood flow fields and distribution patterns of the hemodynamic indices including wall shear stress (WSS) as one of the major hemodynamic parameters of the cardiovascular system and spatial wall shear stress gradient (SWSSG) as an indicator of disturbed flow patterns and hence susceptible sites of lesion developments are analyzed and compared between the two grafts. The tapered 6- to 8-mm graft seemingly is associated with less disturbed flow patterns within the venous anastomosis (VA) and the vein downstream while benefiting from higher blood flow rates within. Also, it shows a definitive advantage in terms of WSS and SWSSG distribution patterns around the VA and throughout the vein downstream with significantly lower values, which reduce the risk of thrombosis formation and stenotic lesion developments. The only disadvantage encountered in using 6- to 8-mm tapered graft is higher values of hemodynamic parameters at the arterial junction attributable to its significantly higher mean blood flow rate within. The results clearly indicate that the tapered 6- to 8-mm graft entirely outperforms straight 6-mm graft hemodynamically as an upper arm hemodialysis vascular access graft and confirms clinical data in the literature, which suggests advantageous use of tapered 6- to 8-mm grafts in the creation of upper arm brachioaxillary hemodialysis vascular access grafts in selected groups of patients with expectably higher patency rates and lower complications.

Keywords Hemodialysis vascular access · Hemodynamics · Computational simulation approach · Thrombosis · Stenotic lesion developments

M. Sarmast · H. Niroomand-Oscuii (✉) · F. Ghalichi
Division of Biomechanics, Department of Mechanical Engineering, Sahand University of Technology, Sahand New Town, Tabriz, Iran
e-mail: niroomand@sut.ac.ir

E. Samiei
School of Engineering, University of British Columbia, Kelowna, BC V1V 1V7, Canada

1 Introduction

Patients on chronic hemodialysis are in dire need of a reliable functional vascular access to their circulatory system able to provide sufficiently high blood flow rates required for efficient hemodialysis treatments. Although arteriovenous (AV) fistulas are the preferred vascular access type for hemodialysis patients due to their greatest longevity, fewest complications, and highest primary and secondary patency rates [1, 2, 22, 30, 39], not every patient is eligible for an AV fistula. Recent trends in the epidemiology of end-stage renal disease (ESRD) show a marked increase in elderly and diabetic patients [1, 43] with higher comorbidities and poorly developed vessels. It can in turn spell the wider usage of the AV grafts (AVGs) as an acceptable alternative for patients in whom AV fistulas are not feasible in the years to come. The major setback associated with the AVGs responsible for

80 % of all hemodialysis access grafts dysfunction is thrombosis due to venous stenosis secondary to venous neointimal hyperplasia at the graft–vein junction or in the draining vein downstream of the VA [1, 2, 15, 39, 52]. It is widely believed that disturbed flow patterns play a key role in the pathogenesis of venous stenosis by triggering intricate biochemical events leading to the onset and progression of intimal hyperplasia (IH) [15, 27, 28, 36]. Disturbed flow manifested in abnormal flow patterns and hemodynamic indices such as high and low wall shear stress [15, 44], temporal and spatial wall shear stress gradients [6, 28, 48, 49], and oscillatory shear index [16] has been widely the subject of numerous studies within the realm of hemodialysis vascular access in order to characterize local hemodynamics at susceptible sites of stenotic lesion formation. Fillinger et al. [11] investigated the impact of graft geometry on the hemodynamics and progression of IH within AV loop grafts in a canine animal study. They suggested that the real causes of hyperplasia in the high flow setting of dialysis access loop grafts are somewhat different than those involved in arterial bypass grafts. Longest and Kleinstreuer [40] conducted a comparative computational study to evaluate hemodynamic conditions in conventional straight and Venaflo^{TM} dialysis access grafts. They reported significant performance improvements in the Venaflo^{TM} graft. Similarly, Kruger et al. [31] demonstrated the positive impact of patch form anastomosis (Venaflo^{TM}) in reducing the incidence of IH in hemodialysis AVGs. Loth et al. [41] analyzed extensively the steady transitional flow patterns at the VA of an AVG by means of in vitro measurements and numerical simulations in addition to a porcine animal study. In vitro comparison of the hemodynamics in 6-mm straight and tapered 4- to 7-mm PTFE AVGs has been investigated by Van Tricht et al. [63] in a pulsatile flow experimental setup. A computational study on the same issue performed by this group revealed no favorable hemodynamic outcome in using 4- to 7-mm tapered grafts [64].

A number of new designs have been proposed and investigated in order to improve the hemodynamic performance of the arterial bypass grafts (ABGs) or AVGs. The impact of S-type grafts on the hemodynamics of ABGs was investigated in an animal study combined with numerical simulations by Fan et al. [10], and the potential impact of a double S-type graft was also suggested by the same group, and more recently, Van Canneyt et al. [60] evaluated the effectiveness of helical configuration AV grafts (SwirlGraft^{TM}) in reducing IH formation in comparison with conventional straight dialysis access grafts and investigated the hemodynamic impacts of the introduction of different helical designs in AVGs [61]. However, there are fundamental questions over the feasibility of these novel graft designs with complex geometries in clinical practice [10, 61].

On the contrary and based on the retrospective and prospective clinical studies in the literature, tapered 6- to 8-mm AVGs are associated with significantly higher patency rates and lower complications when compared to conventional straight 6-mm grafts as upper arm brachioaxillary dialysis access grafts [14, 50]. So, the present study is intended to investigate the hemodynamic impacts of the utilization of tapered 6- to 8-mm graft in the setting of a hemodialysis access loop AVG in order to find out whether there are any hemodynamic advantages accruing from using tapered 6- to 8-mm grafts in comparison with conventional straight 6-mm grafts as hemodialysis AVGs.

To address this goal, an in-depth pulsatile CFD study on three-dimensional models of upper arm brachioaxillary dialysis access loop grafts under physiological flow conditions is presented in order to quantitatively assess the general blood flow features and distribution patterns of the hemodynamic indices in newly created hemodialysis AVGs using the straight 6-mm or tapered 6- to 8-mm grafts. A thorough hemodynamic comparison in terms of velocity fields and well-known hemodynamic indices including wall shear stress (WSS), oscillatory shear index (OSI), and spatial wall shear stress gradient (SWSSG), which is believed to merit further investigation in the realm of AVGs [15], is then made between the grafts.

2 Methods

2.1 Geometry

Three-dimensional models of upper arm loop graft configuration brachioaxillary dialysis access AVGs are acquired using a computer-aided design (CAD) program. The tapered 6- to 8-mm graft is considered to be a long-taper graft type in which the internal diameter of the graft increases gradually from 5 mm at the origin point to 7 mm at the insertion point along the whole length of the graft, and the internal diameter of the straight 6-mm graft is 5 mm throughout its length. It is to be noted that the tapered 6- to 8-mm grafts used in the clinical studies of Polo et al. [50] were of the short-taper graft types in which the diameter of the 8-mm grafts had converted to 6 mm at the arterial anastomosis along 20 mm in length of the graft but as a measure to exclude any possible effect(s) arising from different tapering designs, a long-taper graft type is used in this study. The internal diameter of the brachial artery is assumed 4.25 mm, and the internal diameter of the axillary vein is assumed 6.3 mm in both AVG models, consistent with in vivo measurements [18, 50]. The anastomosis angle is also set to 45° for both the arterial and

venous anastomoses; a conventional anastomosis angle was commonly seen in vascular surgeries and used in a number of previous studies in the field [9, 24, 48, 54, 60–62, 64]. Special care has been taken to develop representative geometries of the AVGs, enabling us to provide a realistic, unbiased comparison of the hemodynamic performance of the straight 6-mm and tapered 6- to 8-mm grafts. The rationale behind choosing the size of the arterial and venous vessels has been so as to provide the critical or near-critical hemodynamic conditions at both the arterial and venous sides of the grafts. According to Polo et al. [50], only patients with axillary veins more than 6 mm in diameter were included in their clinical study and so choosing the veins of 6.3 mm in diameter not only meets this criterion but also represents one of the near-critical hemodynamic conditions at the VA of the grafts. This was also the case in choosing the brachial arteries of 4.25 mm in diameter for both AVG models, which represents one of the lowest possible values in the clinical measurements reported by Hofstra et al. [18]. In the meantime, mean access blood flow rates from the ranges reported by Polo et al. [50] are applied in both AVG models.

A schematic representation of the vascular access model is shown in Fig. 1. The nomenclature used for specific regions of anastomoses is also depicted in an inset to Fig. 1.

2.2 Governing equations and hemodynamic parameters

The governing equations for the three-dimensional incompressible unsteady blood flow are the Navier–Stokes equations as follows:

$$\frac{\partial \vec{u}}{\partial t} + \vec{u}.\nabla\vec{u} = -\frac{1}{\rho}\nabla p + \nu\nabla^2\vec{u} \quad (1)$$

$$\nabla.\vec{u} = 0. \quad (2)$$

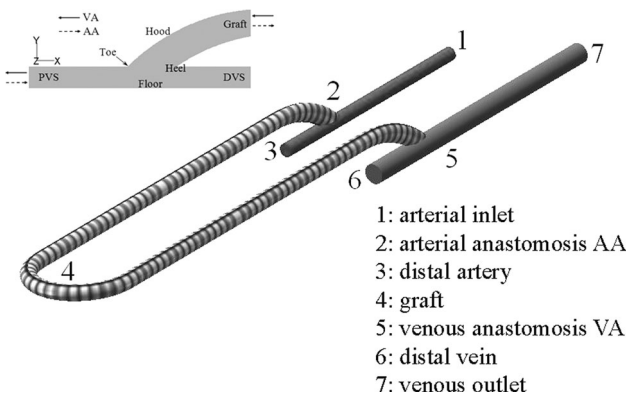

Fig. 1 Schematic representation of the upper arm brachioaxillary dialysis access loop graft. *Inset* shows the nomenclature used for specific regions around the anastomoses; *PVS* and *DVS* are abbreviations for proximal and distal vessel segments, respectively

where ν is the kinematic viscosity of the blood, ρ is the blood density, and $\vec{u} = (u, v, w)$ and p are the three Cartesian components of the velocity vector and pressure, respectively.

The time-averaged and non-dimensional value of the SWSSG is defined as [3]

$$\overline{SWSSG}ND = \frac{d}{\tau_p T}\int_0^T \sqrt{\left(\frac{\partial \tau_x}{\partial x}\right)^2 + \left(\frac{\partial \tau_y}{\partial y}\right)^2 + \left(\frac{\partial \tau_z}{\partial z}\right)^2}\, dt \quad (3)$$

where d is the vessel diameter, T is the period of the cardiac cycle, and τ_p is the Poiseuille WSS at the mean flow rate.

The oscillatory shear index (OSI) is calculated as [16]

$$\mathrm{OSI} = 0.5\left[1 - \frac{\left|\int_0^T \vec{\tau}_w dt\right|}{\int_0^T |\vec{\tau}_w| dt}\right] \quad (4)$$

where $\vec{\tau}_w$ is the instantaneous WSS vector.

2.3 Boundary conditions

The blood is assumed to be a homogeneous, incompressible, and Newtonian fluid with a dynamic viscosity of 3.5 mPa s and a density of 1,050 kg/m^3. The realistically chosen mean blood flow rate at the arterial inlet is 975 ml/min for the straight 6-mm and 1,397 ml/min for the tapered 6- to 8-mm graft in accordance with the measurements reported by Polo et al. [50]. A three-dimensional unsteady laminar blood flow is also assumed within the domain, the vessel walls are considered to be rigid, and no-slip boundary condition is assigned to all rigid walls. Also, it is assumed that the artery and the vein are ligated distal to the anastomoses, i.e., there is no flow through these segments, since the flow in distal parts of the artery and the vein is negligible in comparison with the flow within the graft [46].

In order to better simulate the real physiological conditions within the hemodialysis access grafts, a physiological velocity waveform measured by Kharboutly et al. [25] at the brachial artery of a common hemodialysis patient is assigned as a time-varying parabolic velocity profile at the arterial inlet of the models after mean flow rate adjustment so as to correspond to the above-mentioned mean flow rates. The outlet boundary condition is also a time-dependent pressure waveform measured in an adult human [42]. The inlet and outlet boundary conditions are shown in Fig. 2. The highest Reynolds numbers appeared at the systolic peak (t_1) are approximately 1,572 (1,400–1,572) and 2,205 (2,040–2,205) at the artery and based on the internal diameter of the artery for the straight 6-mm and tapered 6- to 8-mm grafts, respectively.

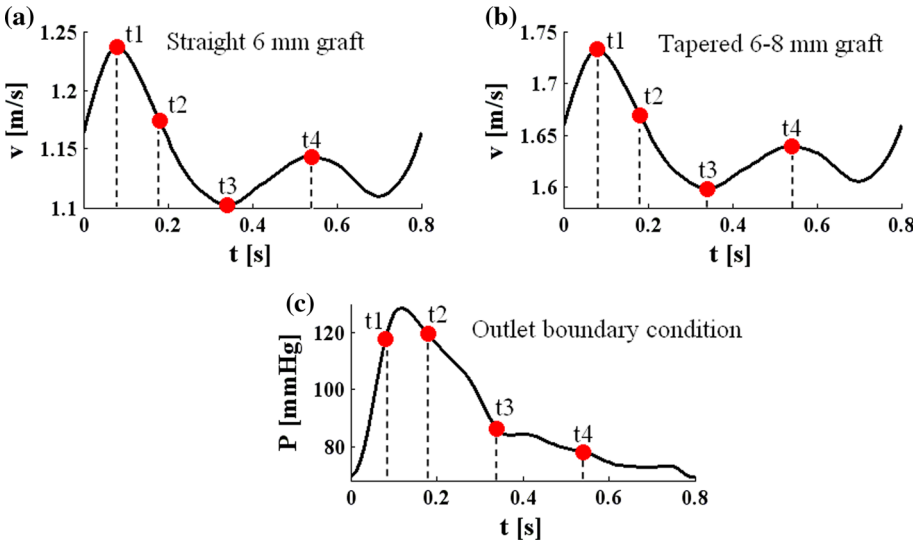

Fig. 2 *Inlet* and *outlet* boundary conditions. **a** Velocity inlet waveform of straight 6-mm graft, **b** velocity inlet waveform of tapered 6- to 8-mm graft, and **c** pressure outlet waveform

2.4 Numerical method

The computational meshes for both models are generated using a specialized grid generation program, Gambit® 2.2.30 (Fluent Inc.). A grid composed of hexahedral elements is implemented in the graft and also proximal parts of the artery and the vein in both models, whereas for arterial and venous anastomoses, tetrahedral elements are employed. Since the wall shear stress distribution is of particular importance in this study and so the accuracy of the velocity fields adjacent to vessel walls, a boundary layer mesh is applied along the vessel walls of the models. A mesh of higher resolution is also applied in the area adjacent to the anastomoses where high variable gradients are expected and detailed flow patterns are important. The final number of mesh elements for each case is selected after performing mesh sensitivity by considering velocity fields, WSS, and pressure values as mesh independency criteria. The total number of meshes applied in the straight 6-mm and tapered 6- to 8-mm AVG models are 2434895 and 2394000 elements, respectively. FLUENT® 6.3.18 (Fluent Inc.), a commercially available CFD code based on finite volume method, is used to solve the governing equations under the aforementioned boundary conditions. Numerical simulations are carried out using a segregated solver with second-order implicit time-stepping formulation. The momentum equations are approximated by second-order accurate discretization scheme, and the velocity–pressure coupling is accomplished via the SIMPLEC algorithm. In order to assign physiological velocity and pressure waveforms at the boundaries and also to calculate SWSSG for post-processing purposes, compiled user-defined functions are developed and hooked to the solver. In order to eliminate any start-up effects of pulsatile flows, the computations are carried out over three full cardiac cycles to obtain stable and accurate periodic solutions. The time-step size is set to 0.5 % of the cardiac cycle, i.e., 4 ms, and the convergence criterion for the continuity and momentum equations at each time step is set to 10^{-6}.

2.5 Model validation

Verification of the present computational model is performed by comparing the numerical prediction of mean pressure distribution with the available experimental measurements on an in vitro model of a vascular access loop graft and also the correspondent numerical results. For this purpose, the same boundary conditions applied by Van Tricht et al. [64] are assigned to the present computational model. The calculated mean pressure distribution across the vascular access model is shown in Fig. 3, which also demonstrates the reference data for comparison. It is to be noted that, due to geometrical differences in terms of the vessel lengths, the displayed curves in Fig. 3 have been displaced in such a way so as to simplify the comparison of the results by locating the anastomoses in a single position. The similarity between the mean pressure distribution patterns is clearly observed in Fig. 3.

3 Results

3.1 Flow patterns

The velocity fields in arterial anastomosis (AA) of the grafts at the peak systolic velocity (t_1) are shown in Fig. 4. The velocity magnitude contour plot and flow field pathlines on the vertical midplane at the AA of the straight graft are presented in Fig. 4a left and right panels, respectively. The blood flow from the proximal artery accelerates

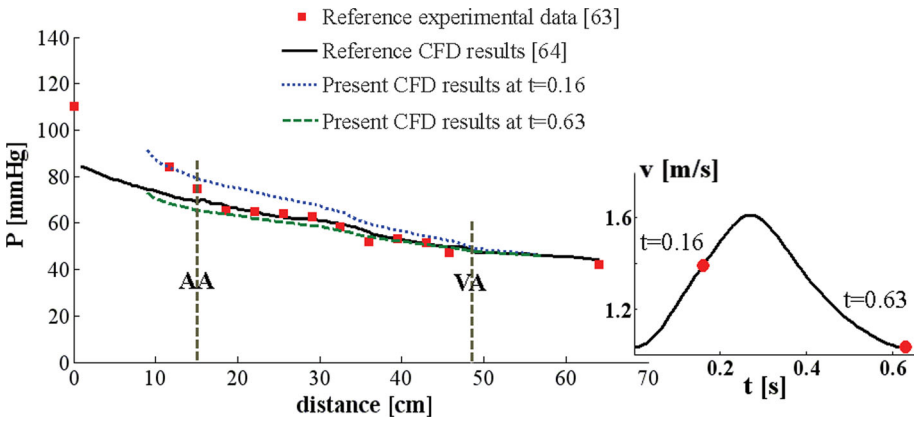

Fig. 3 Calculated mean pressure distribution along the vascular access model together with the experimental and computational reference data [63, 64]

through the graft at the AA colliding into the graft wall near the anastomosis heel. The maximum velocity observed at the graft entrance is 2.02 m/s. From the pathlines of the flow field, a region of flow recirculation can be identified at the graft hood adjacent to the anastomosis. The formation of a second vortex in distal segment of the artery is also clearly observed. Figure 4b represents the axial (*x*-direction) velocity magnitude contours in addition to the in-plane velocity vectors in several transverse planes along the AA of the straight 6-mm graft. In cross-sectional plane 10 mm proximal to the AA (X = −10), the flow is completely fully developed without in-plane velocity component. Regions with negative axial velocity magnitudes at the middle of the AA (X = 0) correspond to the formation of the previously mentioned vortices at this location. The in-plane velocity vectors in the cross-sectional plane 5 mm distal to the AA (X = 5) clearly show the existence of nearly symmetrical vortices at this section of the graft. Further downstream (X = 20), the in-plane velocity vectors are suggestive of the reduction in the vortical flow intensity in the graft.

Very similar flow patterns are observed at AA of the tapered graft (Fig. 4c, d) with maximum velocities being increased by approximately 35 % and so stronger the vortices generated at the AA of this graft.

Flow patterns at the VA of the grafts at peak systolic velocity (t_1) are also shown in Fig. 5. The blood flow within the graft enters the recipient vein at the VA colliding into the graft hood. Within the anastomosis, there is a significant skewing of the velocity toward the vein floor with a stagnation point on the vein floor opposite the graft outflow. The maximum velocity observed at the exit of the graft on the vertical midplane of the VA is 1.71 and 1.46 m/s for straight and tapered grafts, respectively, in spite of almost 40 % higher blood flow rate in tapered 6- to 8-mm graft.

A vortical flow pattern is developed within whole diameter of the ligated end of the vein just distal to the stagnation point. Flow separation and a recirculation region are also observed along the upper wall surface of the vein just downstream to the VA in both grafts (Fig. 5a, c), which is smaller in case of tapered 6- to 8-mm graft.

Axial velocity magnitude contours in addition to in-plane velocity vectors in several transverse planes along the VA of the grafts (Fig. 5b, d) show that nearly symmetric vortices rotating in the opposite directions are formed downstream of the VA which are still present 20 mm downstream. These vortices are initially formed along the lateral walls of the vein and gradually shift toward the vein center with increasing distance from the anastomosis. The flow is less skewed and much more aligned with the vein downstream within the VA and smoother and less disturbed in proximal vein of the tapered 6- to 8-mm graft.

The above-mentioned characteristic features of the flow at both anastomoses are generally observed through most of the cardiac cycle (t_2–t_4).

3.2 Pressure drop

The calculated mean pressure distribution across the vascular access model is plotted in Fig. 6 for both grafts. As is evident in Fig. 6, the tapered 6- to 8-mm graft is associated with higher pressure drops both in rate and magnitude along the proximal segments of the artery and the vein due to its higher blood flow rate within. Also, the pressure drop within the tapered 6- to 8-mm graft is significantly lower than the straight 6-mm graft due to gradual pressure recovery within the tapered graft.

3.3 Vorticity magnitude

The area-weighted average values of the vorticity magnitude at successive planes along the venous side of the AVGs are plotted in Fig. 7 at peak systolic velocity (t_1). As it can be seen in Fig. 7, both AVG models show a similar trend with regard to the vorticity magnitude across the VA and the vein downstream. As expected, the tapered 6- to

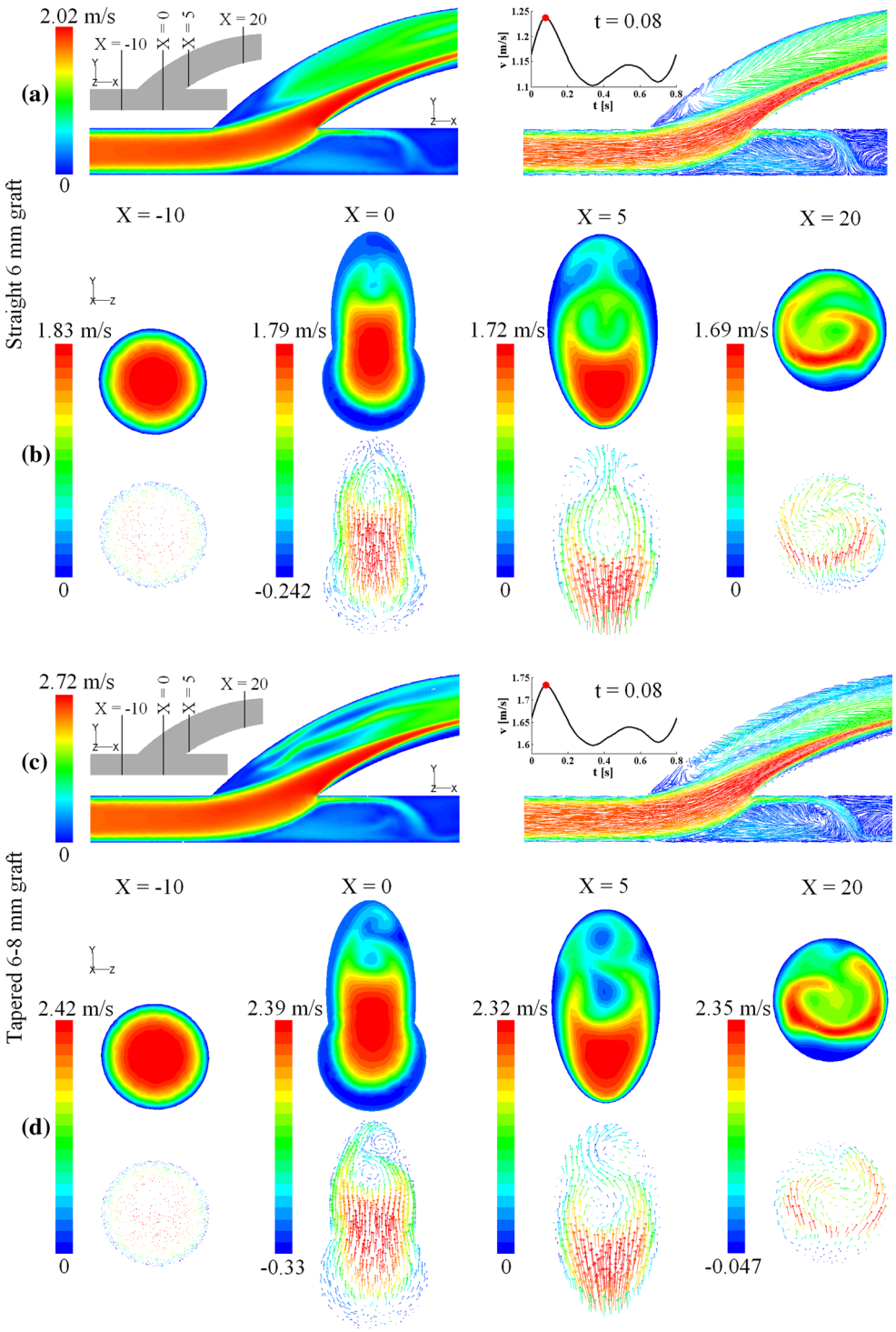

Fig. 4 Velocity fields in AA of the grafts. **a** Vertical midplane, straight 6-mm graft; **b** transverse planes, straight 6-mm graft; **c** vertical midplane, tapered 6- to 8-mm graft; **d** transverse planes, tapered 6- to 8-mm graft

8-mm graft is associated with lower vorticity magnitudes within the VA and the vein downstream adjacent to the VA due to lower velocity magnitudes observed at the exit of the tapered 6- to 8-mm graft (cf. Fig. 5) irrespective of its significantly higher blood flow rate. As flow develops further downstream within the proximal vein and almost 25 mm proximal to the anastomosis toe, the mean vorticity magnitude values of the tapered 6- to 8-mm graft exceed the vorticity magnitude values of the straight 6-mm graft.

3.4 Hemodynamic parameters

Wall shear stress (WSS) contour plots around the AA of the grafts at the peak systolic velocity are represented in Fig. 8.

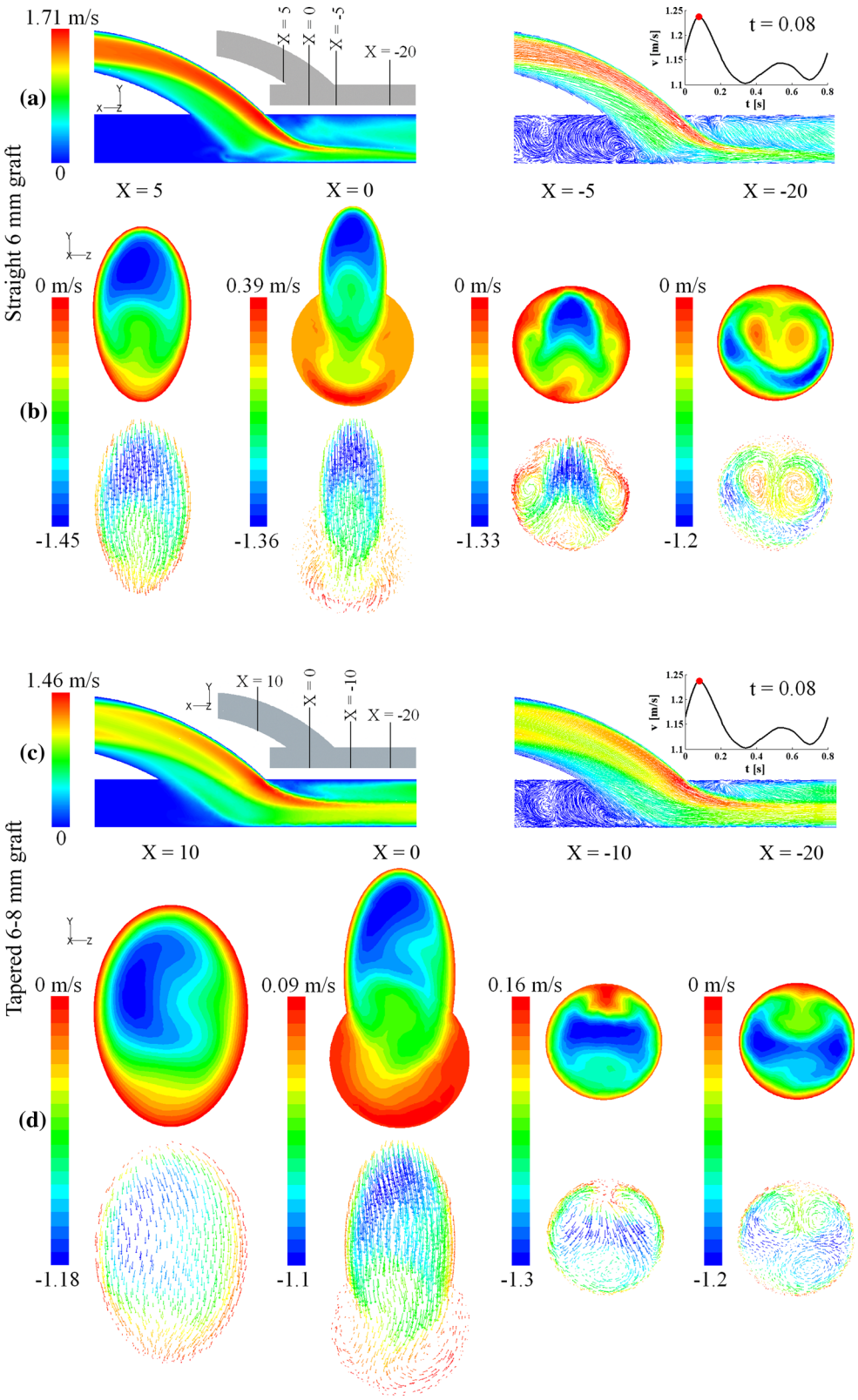

Fig. 5 Velocity fields in VA of the grafts. **a** Vertical midplane, straight 6-mm graft; **b** transverse planes, straight 6-mm graft; **c** vertical midplane, tapered 6- to 8-mm graft; **d** transverse planes, tapered 6- to 8-mm graft

The WSS distribution pattern at the AA is quite similar for both grafts with peak values occurring along a little crescent shape distance on the heel side of the suture line (with the magnitude of 98 Pa for straight and 157 Pa for tapered graft). Similar WSS distribution patterns appear around AA of the grafts at different time levels of the cardiac cycle (t_2–t_4).

Wall shear stress (WSS) contour plots around the VA of the grafts are also shown in Fig. 9 at four typical time levels of the cardiac cycle (t_1–t_4). The WSS contours around the VA of the straight 6-mm graft (Fig. 9a) show high shear stress regions at the anastomosis toe in the range 36–45 Pa at all time levels and the lateral wall surfaces of the proximal vein around the stagnation point extending further downstream in accordance with the vortices appeared along the lateral walls of the downstream vein (Fig. 5b).

The WSS distribution pattern around the VA of the tapered 6- to 8-mm graft shows just a tiny high shear stress region around 0.47 mm^2 along the perimeter of the VA at the toe (cf. Fig. 9) in the range 38–50 Pa, on the graft side of the anastomosis throughout the cardiac cycle (t_1–t_4). The lateral wall surfaces of the proximal vein downstream to the anastomosis only experience moderate WSS values limited to 29 Pa, and also a smaller low shear stress region is observed along the upper wall surface of the downstream vein indicative of a more uniform WSS distribution and consequently better washout of blood residing near the wall that lowers the risk of thrombosis formation at this site of the vein in tapered 6- to 8-mm graft. It is also evident that the stagnation point is either nonexistent or not well defined at the VA of the tapered 6- to 8-mm graft. For all time levels (t_1–t_4), a broadly similar WSS distribution pattern is observed around the VA in both grafts with lower abnormal WSS values in favor of the tapered 6- to 8-mm graft.

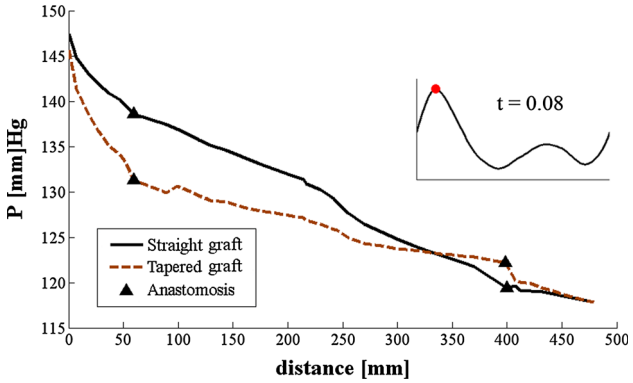

Fig. 6 Mean pressure distribution along the vascular access for both grafts

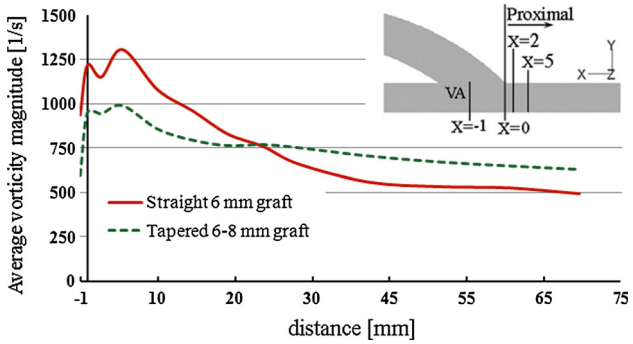

Fig. 7 Average vorticity magnitude along the venous side of the AVGs (X = −1 denotes the mid-anastomosis location in both AVG models)

Figure 10 shows the distribution patterns of the SWSSG around the AA and VA of the grafts. The SWSSG contours at the AA of both grafts being very resemblant to the WSS contours show similar patterns with peak SWSSG values (270 for tapered vs. 220 for straight) occurring at several distinct small regions on the arterial upper wall near the heel and along the suture line.

The distribution of the SWSSG at the VA of the straight 6-mm graft demonstrates regions of elevated SWSSG values up to 306 along the lateral wall surfaces of the downstream vein similar to the WSS distribution pattern observed in this region of this graft (Fig. 9a). SWSSG values at the toe, heel, along the suture ring, and the vein floor across VA are in the ranges 122–165, 140–183.5, 73–116, and 130–175, respectively. The SWSSG contours around VA of the tapered 6- to 8-mm graft show remarkably lower values limited to 134 in much smaller extent of the vessel wall surface areas over the entire VA region. SWSSG values at the toe, heel, and along the suture ring are in the ranges 68–102, 45–55, and 15–36, respectively. Furthermore, nearly all of the high SWSSG values on the vein floor are eliminated in tapered 6- to 8-mm graft.

The OSI as defined in Eq. 4 is plotted in Fig. 11 around the VA of the grafts. The largest OSI values, i.e., the values close to 0.5, appeared only on distal vein segments of the grafts with minimal differences. As it can be observed in Fig. 11, OSI is almost absent in the graft, the vein across the junction, along the suture ring, and also the whole

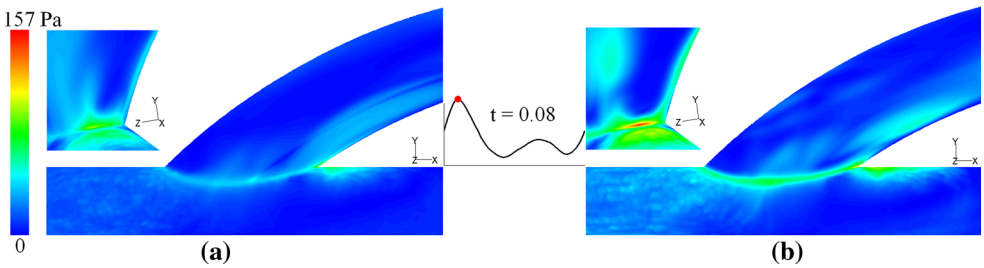

Fig. 8 WSS contour plots around the AA of the grafts at the systolic peak. **a** Straight 6-mm graft; **b** tapered 6- to 8-mm graft

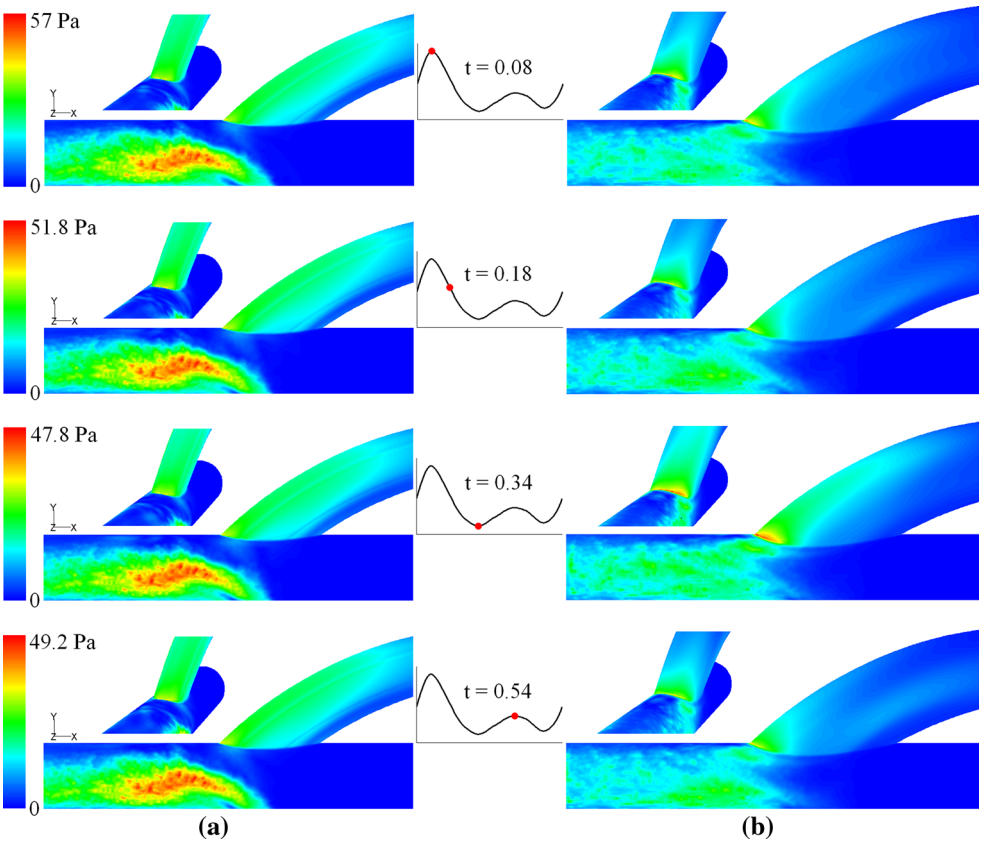

Fig. 9 WSS contour plots around the VA of the grafts. **a** Straight 6-mm graft; **b** tapered 6- to 8-mm graft

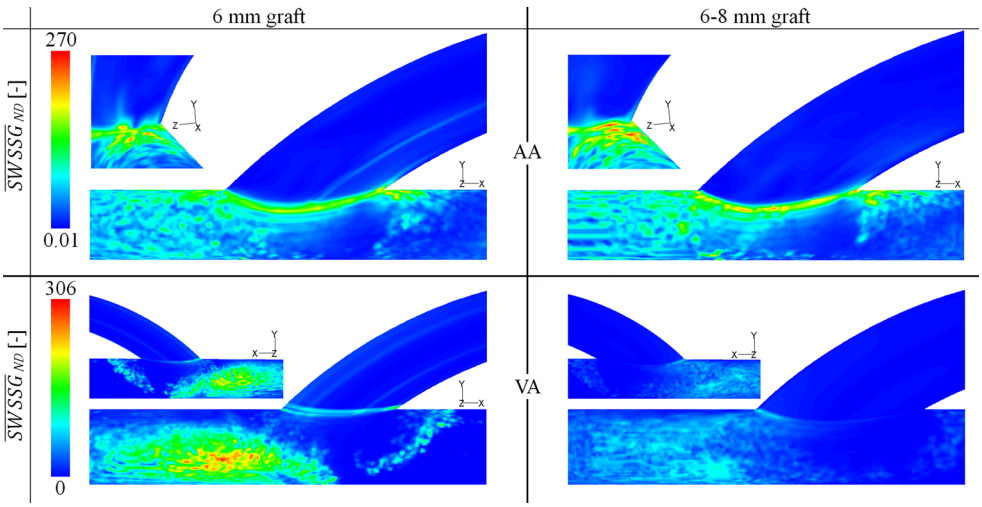

Fig. 10 SWSSG contour plots around the AA (*top panel*) and across the VA (*bottom panel*) of the grafts

proximal vein region in tapered 6- to 8-mm graft, and only relatively large OSI values in the range 0.1–0.23 appear on the upper wall surface of the vein a short distance from the toe corresponding to the formation of a recirculation region at this site of the vein. The OSI contours for straight 6-mm graft are almost similar to the tapered graft with slightly larger extended nonzero OSI regions and higher magnitudes in the range 0.13–0.29, indicative of more changes in flow direction at this site of the vein. Also, additional nonzero OSI regions with the magnitudes in the range 0.14–0.21 are observed in the lateral sides of the VA across the junction in straight 6-mm graft.

4 Discussion

Prospective and retrospective randomized clinical trials have demonstrated interestingly higher primary and

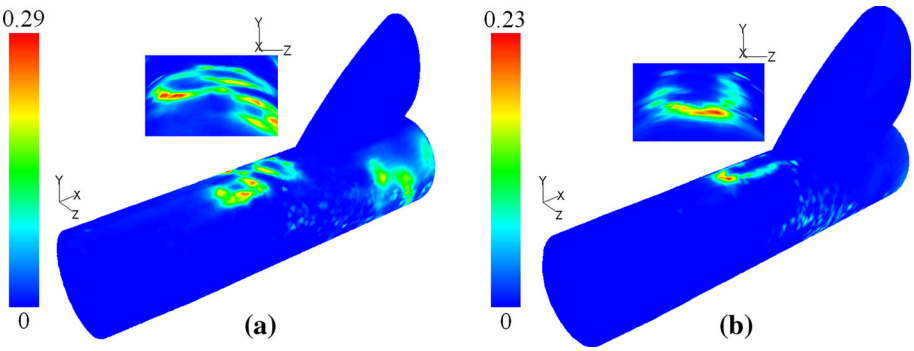

Fig. 11 OSI contour plots across the VA of the grafts. **a** Straight 6-mm graft; **b** tapered 6- to 8-mm graft

secondary patency rates for tapered 6- to 8-mm grafts in comparison with straight 6-mm grafts (85 vs. 62 % and 78 vs. 58 % 1 and 2 years, respectively) [14, 50].

To date, to the best of the authors' knowledge, there is no published data with regard to the hemodynamics of tapered 6- to 8-mm graft irrespective of its superior patency and lower complication rates in comparison with straight 6-mm graft as upper arm hemodialysis vascular access graft. Thus, the present study was set up to assess the hemodynamic performance of each of these grafts.

The results of the present study indicate broadly similar velocity fields and hemodynamic indices distribution patterns around AA of the grafts. Extremely high and non-physiological WSS values are observed around the AA in both grafts with higher magnitudes belonging to the tapered 6- to 8-mm graft. These WSS values exceed profoundly the activation threshold for leukocytes (shear stress levels of between 7.5 and 15 Pa for 10 min) [5] and platelets (>10 Pa for 1 min) [56] in both grafts. The exposure of red blood cells to shear stresses above 250 Pa may also induce hemolysis [58]. It is worth noting that although the maximum WSS values reaches to 146–157 Pa around the AA of the tapered 6- to 8-mm graft over the cardiac cycle, much closer to the lysis threshold than the values in straight 6-mm graft, but this only occurs along a very limited crescent-shaped distance at the heel side of the suture line. The major differences in these grafts lie at the VA where tapered 6- to 8-mm graft seemingly is associated with less disturbed flow patterns within the anastomosis and the vein downstream. The larger diameter of the tapered 6- to 8-mm graft at the VA let the graft conforms better to the host vein and so smaller the flow disturbances as the blood flow enters the vein and better the hemodynamic condition at the VA and the vein downstream.

Area-weighted average values of the hemodynamic parameters are calculated over the successive blocks 2 mm in length on the venous wall surface along a distance of almost 2 cm proximal to the toe. The results are presented as bar charts in Fig. 12. From these charts, it is obvious that both the WSS and SWSSG values are lower in tapered 6- to 8-mm graft, with much discernible differences in SWSSG

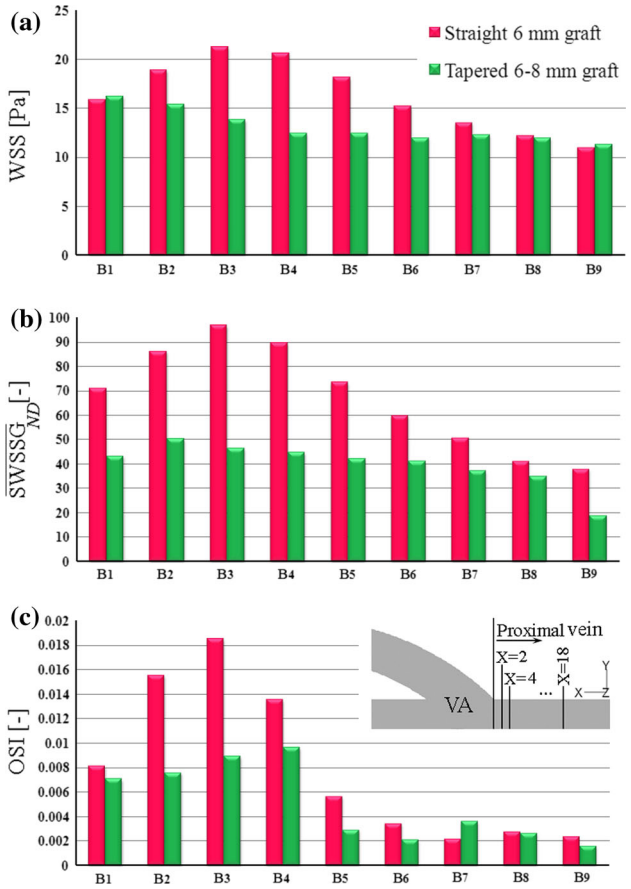

Fig. 12 Comparison of area-weighted averaged hemodynamic indices at the proximal vein. B1 through B9 represent the first through the ninth block in succession from *right* to *left* as shown in inset

distribution bar charts. A similar trend is also observed in OSI distribution bar charts (Fig. 12c) consistent with the observation of larger extended nonzero OSI regions with higher magnitudes in Fig. 11.

It is worth to mention that the aforementioned hemodynamic values should not be considered as absolute values for hemodynamic indices but more as indicative values which fulfill suitably the comparative purposes of this study.

Also, as pointed out by Van Tricht et al. [65], the WSS values above 35 Pa should be addressed in studies encountered with the evaluation of WSS distribution in association with IH developments and it has been shown that platelet activation and thrombosis formation require high shear stress values of at least 31.5 Pa and above [21]. While the entire surface of the downstream vein in tapered 6- to 8-mm graft is subjected to WSS values (<29 Pa) below the aforementioned thresholds except for a very small spot at the toe, the WSS values exceed profoundly both these limits in the downstream vein of the straight 6-mm graft (Fig. 9a).

A plethora of hemodynamic indices have been implicated in the initiation and development of IH, but all of them are originally from the context of arterial bypass graft irrespective of the substantial differences between the hemodynamic characteristics of ABGs and AVGs [15]. High wall shear stress values are thought to cause endothelial damage [13, 20] as well as the damages to the blood-borne particles [5, 21, 56, 58] and thrombosis formation [21, 56]. On the other hand, extremely low wall shear stress values [44, 53] and particularly low and oscillatory wall shear stress values [23, 32] are correlated with intimal thickening and hence development of intimal hyperplasia in ABG anastomoses.

The SWSSG is also believed to be a major hemodynamic indicator of disturbed flow patterns and hence susceptible sites of IH developments in several studies [28, 36, 37], and there are a number of in vitro studies in the literature with regard to the implications of high SWSSG magnitudes on the morphological and functional changes in the endothelium and so its correlation with sites of lesion developments; DePaola et al. [4] demonstrated the impacts of large SWSSG-induced morphological and functional changes in the endothelium that might contribute to occlusive lesion developments. Ojha [48] suggested the correlation between the host artery floor IH and the large SWSSGs. In vitro studies of Tardy et al. [59] and Nagel et al. [45] indicated that local SWSSG plays a key role in the morphologic remodeling of the vascular endothelium in vivo. Flow visualization studies of Leask et al. [33] in realistic models of coronary artery bypass grafts replicated by postmortem casting also indicated that high SWSSGs are likely factors of IH growth on the sharp hood curvature of bypass grafts. More recently, Rouleau et al. [51] showed the dependence of endothelial cell morphology on SWSSG in an in vitro experimental setup replicating an atherosclerotic region, and Steinman et al. [57] indicated that the onset of IH formation could be attributed to the elevated SWSSG magnitudes.

Fillinger et al. [11] questioned the suitability of several hemodynamic predictors including low shear stress values in correlation with sites of lesion development and suggested that the real causes of IH in the high flow setting of dialysis access loop grafts are somewhat different than those involved in ABGs. Haruguchi et al. [15] supported this idea, denoting that no important IH has been observed in areas of low WSS in the high flow setting of AVGs. They speculated that, in AVGs, IH is most likely to develop in sites markedly different from those in which it usually occurs in ABGs and they postulated that in AVGs, high WSS causes IH.

Furthermore, the elevated mean blood flow rate within the AV vascular accesses gives rise to a reduced pulsatility index compared to the normal arterial flows [8, 26, 40, 41, 55] and so Longest and Kleinstreuer [40] speculated that the oscillatory shear index may not be an effective hemodynamic parameter in studies with regard to the AVGs with their mildly varying input pulse. Kharboutly et al. [26] also found a null OSI throughout the length of the vessel when a physiological blood flow condition was applied in their patient-specific CFD model of an AVF. Ene-Iordache et al. [8] also reported very low OSI magnitudes (0.075) at the heel side of the vein in a simplified model of an end-to-side AVF compared to the significantly higher OSI values observed on the anastomosis floor and on the lateral wall of the distal artery, in contradiction to the clinical evidences on frequent sites of stenotic lesion developments. As discussed earlier, the results of the present study did not show a significant difference between the grafts in this regard, with the most vessel wall surfaces of the models subjected to OSI values below 0.1 at the venous side of the AVGs.

Also, in the present study, in line with the previous patient-specific [7, 26] and CFD studies in the realm of hemodialysis arteriovenous vascular accesses [62, 64], we found that both AVG models are mostly subjected to high wall shear stress values at the VA and the vein downstream with less significant low shear stress regions, given the upper limit wall shear stress values of the low shear stress theory, i.e., wall shear stress values below 0.2 Pa [44] or even 1 Pa [53]. As it can be seen in Fig. 9, only a limited fraction of the lateral wall surface of the vein along the distal half of the VA, as well as the distal half of the suture ring and distal parts of the vein wall surface, experiences WSS values below 1 Pa in both AVG models. The only difference between the AVG models in this regard lies at the upper wall surface of the vein downstream to the VA where a small low shear stress region (below 1 Pa) can be identified in straight 6-mm AVG model that extends as several spot regions from 2 mm proximal to the anastomosis toe for almost 4 mm throughout the cardiac cycle but it is almost nonexistent in tapered 6- to 8-mm graft except a very small spot-like region 6 mm proximal to the anastomosis toe, representative of a better washout of blood residing near the upper wall of the proximal vein in tapered 6- to 8-mm graft.

Therefore, it is expected that the relative residence time (RRT) parameter [17], which characterizes both low and oscillating shear in tandem and is believed to be a robust single metric of low and oscillating shear in the context of carotid bifurcation hemodynamics [34], would not be a descriptive hemodynamic predictor in the generally low-oscillating, high-shear AVG models under investigation, and our results confirm this speculation as the RRT contour plots (not shown) show RRT values below 0.01 for nearly whole the vessel wall surfaces around the VA and the vein downstream for both grafts.

Figure 13 represents a qualitative comparison between the quantitative measurements of IH thickness across the vein of a loop AVG in an animal study conducted by Fillinger et al. [11] with the hemodynamic data of the present study using the same subdivision of the reference study as shown in an inset to Fig. 13. It is to be noted that, however, the blood flow conditions are not exactly the same between these two studies but this comparison at least provides some insight into in vivo IH distribution in a high flow setting of an AV loop graft, and let us evaluate the adequacy of the hemodynamic parameters in identification of sites susceptible to IH formation by confronting the acquired hemodynamic data of the present study with the histological findings of Fillinger et al. [11]. It is also worth mentioning that the mean volumetric blood flow rates are quite similar and of the same order between these two studies (1,040 ± 120 and 1,340 ± 140 cc/min in the reference study vs. 975 ml/min in the present study).

From Fig. 13, WSS distribution correlates well with measured venous IH thickness pattern, in agreement with the prediction of progressive dissipation of flow disturbances in moving away downstream from the anastomosis [11]. This is also the case with the OSI distribution pattern notwithstanding, much more discernible difference in hemodynamic values at locations L1 and L2 (Fig. 13d).

Lower values of the hemodynamic parameters at Sects. 4 and 5 (Fig. 13b, c) are also consistent with the reported little or no IH developments at these sections of the AVGs [11] but higher OSI magnitude observed at location L5 contrasts this trend.

The higher SWSSG magnitude observed downstream to the VA (cf. locations L1 and L2 in Fig. 13c) does not correlate with in vivo observation of IH distribution pattern (cf. locations L1 and L2 in Fig. 13a) due to a fact that is not reflected in WSS distribution bar charts. From Figs. 9, 10, and 11, it is obvious that the values of the hemodynamic parameters increase initially along the proximal vein and then decrease as distance from the anastomosis increases. This trend is not mentioned in the reference animal study [11], attributable to the paucity of the points applied for data acquisition in that study or the geometrical and hemodynamic differences between these two studies. Such

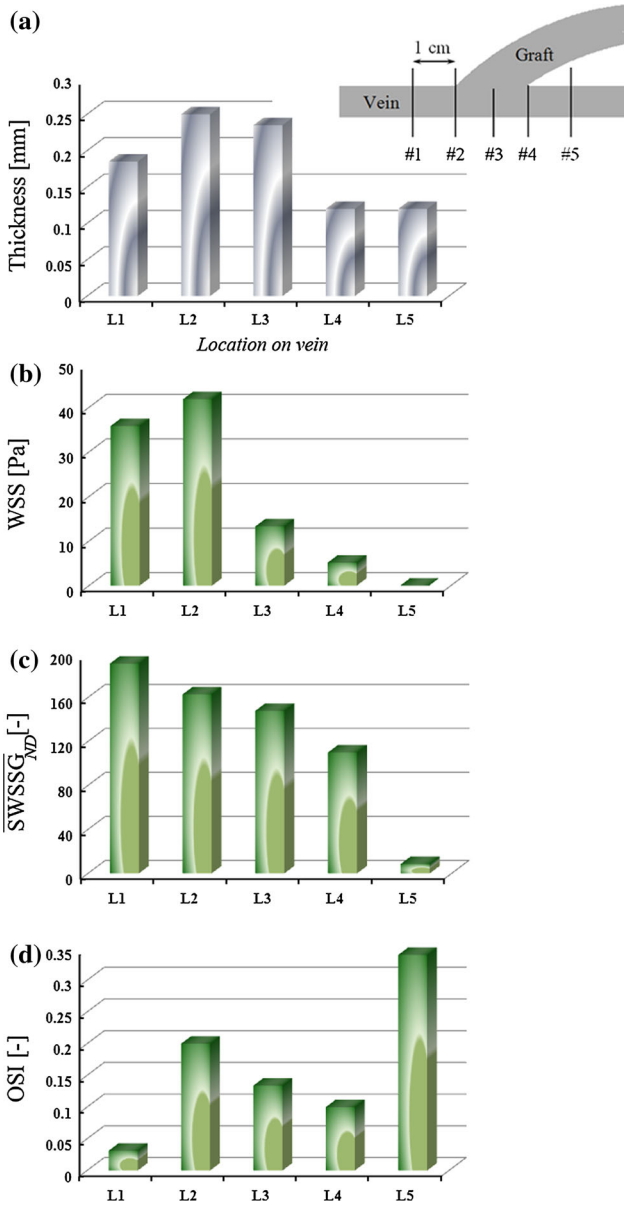

Fig. 13 Comparison of segmental magnitudes of the hemodynamic indices **b**, **c** with venous intimal-medial thickness measurements [11] in straight 6-mm grafts **a**, L1 through L5 refer to locations 1 through 5 as shown in inset

a correlation has yet to be clarified in humans in further research.

It should be pointed out that in the present CFD study on the hemodynamic performance of the straight 6-mm and tapered 6- to 8-mm grafts, idealized geometries were used to catch the general blood flow features and distribution patterns of the hemodynamic indices in newly implanted hemodialysis AVGs under physiological flow conditions. The arterial and venous vessel segments were uniformly circular. The artery, the graft, and the vein were completely straight and symmetric about the centerline plane. The elliptic-shaped AA and VA were also both symmetric

around the centerline plane and planar, i.e., the artery and the graft at the AA and the graft and the vein at the VA lay in the same plane without any non-planarity. The vessel walls were also assumed to be rigid, and the blood was considered to be a Newtonian fluid. We expect the rigid wall assumption to be reasonable, at least as far as the VA and the vein downstream are at stake, since veins have low compliance at arterial pressures and the commercially available stretch PTFE grafts are also known to have even smaller compliance at these pressures [35, 41].

However, the rigid wall assumption might be considered as the main shortcoming of this model but there are evidences that the occurrence of stenoses in prosthetic AV grafts in or adjacent to the VA cannot be associated with compliance mismatch [19]. The assumption of a Newtonian fluid also seems to be reasonable due to the pulsatile high blood flow rate and hence high rates of shear in the AVG models under investigation [47]. Moreover, it has been shown that the rigid wall and the Newtonian fluid assumptions have a minor effect on the overall flow patterns as Friedman et al. [12] suggested that there is no significant effect on the slopes of the correlations between intimal thickness and any normalized wall shear rate measure.

While the variability of the hemodialysis vascular access graft geometry in terms of possible bends or torsions in the graft, luminal area, and angle of insertion variations at both the arterial and venous sides as well as different blood flow conditions among patients would affect the hemodynamic condition of the single subject in a patient-specific study and needs to be investigated in further research, we believe that the present study can well represent the general blood flow patterns and common hemodynamic indices distribution in a typical setting of a newly implanted hemodialysis vascular access graft that enables us to provide an unbiased comparison between the hemodynamic performance of the conventional straight 6-mm and tapered 6- to 8-mm grafts.

The tapered 6- to 8-mm graft was associated with less disturbed blood flow patterns at the VA and the vein downstream, and as glaringly illustrated in hemodynamic indices distribution patterns, it exhibits significantly better hemodynamic performance in terms of WSS and SWSSG distribution patterns.

From the clinical perspective, high access blood flow may prolong the lifetime of dialysis access grafts by further retarding low flow-induced access thrombosis. On the other hand, high access blood flow in tandem with several other risk factors such as female gender, age over 60, diabetes mellitus, and arterial occlusive diseases can induce ischemic steal syndrome by compromising the supply of blood flow to distal tissues of the extremity [29, 38].

So, as pointed out by Polo et al. [50], appropriate selection of patients to receive 6- to 8-mm tapered grafts via preoperative evaluation may result in exploiting both the higher access blood flows and also better hemodynamic condition at the venous side, which can in tandem spell the longer lifetimes of these grafts.

5 Conclusion

The current CFD study presents the pulsatile simulations of 3D hemodialysis vascular access grafts of different diameters: 6-mm straight and tapered 6–8 mm under physiological boundary conditions. The particular differences in the grafts lie in the VA region and the vein downstream where IH has been documented to occur.

The larger diameter of the tapered graft at the VA let the blood flow align well with the host vessel and so less disturbed blood flow patterns are observed within the VA and the vein downstream. The overall magnitudes of hemodynamic indices are also greatly reduced throughout the VA region in tapered 6- to 8-mm graft with significantly better distribution patterns in comparison with the straight 6-mm graft.

The results clearly demonstrate that the tapered 6- to 8-mm graft entirely outperforms straight 6-mm graft hemodynamically as a hemodialysis vascular access graft and confirm clinical data that suggest advantageous use of tapered 6- to 8-mm grafts in creation of upper arm brachioaxillary dialysis access grafts. The findings of this study have implications for clinical practice guidelines and also in making a room for further researches on improvements in design of the optimal graft diameters.

References

1. Akoh JA (2009) Prosthetic arteriovenous grafts for hemodialysis. J Vasc Access 10:137–147
2. Allon M (2007) Current management of vascular access. Clin J Am Soc Nephrol 2:786–800
3. Buchanan JR, Kleinstreuer C, Hyun S, Truskey GA (2003) Hemodynamics simulation and identification of susceptible sites of atherosclerotic lesion formation in a model abdominal aorta. J Biomech 36:1185–1196
4. DePaola N, Gimbrone MA Jr, Davies PF, Dewey CF Jr (1992) Vascular endothelium responds to fluid shear stress gradients. Arterioscler Thromb 12(11):1254–1257
5. Dewitz TS, McIntire LV, Martin RR, Sybers HD (1979) Enzyme release and morphological changes in leukocytes induced by mechanical trauma. Blood Cells 5(3):499–512
6. El Zahab Z, Divo E, Kassab A (2010) Minimisation of the wall shear stress gradients in bypass grafts anastomoses using meshless CFD and genetic algorithms optimization. Compu Methods Biomech Biomed Engin 13(1):35–47
7. Ene-Iordache B, Mosconi L, Remuzzi G, Remuzzi A (2001) Computational fluid dynamics of a vascular access case for hemodialysis. J Biomech Eng 123(3):284–292

8. Ene-Iordache B, Remuzzi A (2012) Disturbed flow in radial-cephalic arteriovenous fistulae for haemodialysis: low and oscillating shear stress locates the sites of stenosis. Nephrol Dial Transplant 27(1):358–368
9. Ethier CR, Prakash S, Steinman DA et al (2000) Steady flow separation in a 45 degree junction. J Fluid Mech 411:1–38
10. Fan Y, Xu Z, Jiang W et al (2008) An S-type bypass can improve the hemodynamics in the bypassed arteries and suppress intimal hyperplasia along the host artery floor. J Biomech 41:2498–2505
11. Fillinger MF, Reinitz ER, Schwartz RA, Resetarits DE, Paskanik AM, Bruch D, Bredenberg CE (1990) Graft geometry and venous intimal-medial hyperplasia in arteriovenous loop grafts. J Vasc Surg 11:556–566
12. Friedman MH, Bargeron CB, Duncan DD, Hutchins GM, Mark FF (1992) Effects of arterial compliance and non-Newtonian rheology on correlations between intimal thickness and wall shear. J Biomech Eng 114(3):317–320
13. Fry DL (1968) Acute vascular endothelial changes associated with increased blood velocity Gradients. Circ Res 22:165–197
14. Garcia-Pajares R, Polo JR, Flores A, Gonzalez-Tabares E, Solis JV (2003) Upper arm polytetrafluoroethylene grafts for dialysis access: analysis of two different graft sizes: 6 mm and 6–8 mm. Vasc Endovasc Surg 37:335–343
15. Haruguchi H, Teraoka S (2003) Intimal hyperplasia and hemodynamic factors in arterial bypass and arteriovenous grafts: a review. J Artif Organs 6:227–235
16. He X, Ku DN (1996) Pulsatile flow in the human left coronary artery bifurcation: average conditions. J Biomech 118(1):74–82
17. Himburg HA, Grzybowski DM, Hazel AL et al (2004) Spatial comparison between wall shear stress measures and porcine arterial endothelial permeability. Am J Physiol Heart Circ Physiol 286(5):H1916–H1922
18. Hofstra L, Bergmans DC, Hoeks AP, Kitslaar PJ, Leunissen KM, Tordoir JH (1994) Mismatch in elastic properties around anastomoses of interposition grafts for hemodialysis access. J Am Soc Nephrol 5(5):1243–1250
19. Hofstra L, Bergmans DC, Leunissen KM et al (1995) Anastomotic intimal hyperplasia in prosthetic arteriovenous fistulas for hemodialysis is associated with initial high flow velocity and not with mismatch in elastic properties. J Am Soc Nephrol 6(6):1625–1633
20. Hofstra L, Bergmans DC, Leunissen KM et al (1996) Prosthetic arteriovenous fistulas and venous anastomotic stenosis: influence of a high flow velocity on the development of intimal hyperplasia. Blood Purif 14(5):345–349
21. Holme PA, Orvim U, Hamers MJ, Solum NO, Brosstad FR, Barstad RM, Sakariassen KS (1997) Shear-induced platelet activation and platelet microparticle formation at blood flow conditions as in arteries with a severe stenosis. Arterioscler Thromb Vasc Biol 17(4):646–653
22. Huber TS, Carter JW, Carter RL, Seeger JM (2003) Patency of autogenous and polytetrafluoroethylene upper extremity arteriovenous hemodialysis accesses: a systematic review. J Vasc Surg 38:1005–1011
23. Keynton RS, Evancho MM, Sims RL, Rodway NV, Gobin A, Rittgers SE (2001) Intimal hyperplasia and wall shear in arterial bypass graft distal anastomoses: an in vivo model study. J Biomech Eng 123(5):464–473
24. Keynton RS, Rittgers SE, Shu MC (1991) The effect of angle and flow rate upon hemodynamics in distal vascular graft anastomoses: an in vitro model study. J Biomech Eng 113(4):458–463
25. Kharboutly Z, Deplano V, Bertrand E, Legallais C (2010) Numerical and experimental study of blood flow through a patient-specific arteriovenous fistula used for hemodialysis. Med Eng Phys 32(2):111–118
26. Kharboutly Z, Fenech M, Treutenaere JM, Claude I, Legallais C (2007) Investigations into the relationship between hemodynamics and vascular alterations in an established arteriovenous fistula. Med Eng Phys 29(9):999–1007
27. Kleinstreuer C, Hyun S, Buchanan JR, Longest PW, Archie JP, Truskey GA (2001) Hemodynamic parameters and early intimal thickening in branching blood vessels. Crit Rev Biomed Eng 29(1):1–64
28. Kleinstreuer C, Lei M, Archie JP Jr (1996) Flow input waveform effects on the temporal and spatial wall shear stress gradients in a femoral graft-artery connector. J Biomech 118(4):506–510
29. Knox RC, Berman SS, Hughes JD, Gentile AT, Mills JL (2002) Distal revascularization-interval ligation: a durable and effective treatment for ischemic steal syndrome after hemodialysis access. J Vasc Surg 36:250–256
30. Konner K et al (2003) The arteriovenous fistula. J Am Soc Nephrol 14:1669–1680
31. Krueger U, Zanow J, Scholz H (2002) Computational fluid dynamics and vascular access. Artif Organs 26(7):571–575
32. Ku DN, Giddens DP, Zarins CK, Glagov S (1985) Pulsatile flow and atherosclerosis in the human carotid bifurcation. Positive correlation between plaque location and low oscillating shear stress. Arteriosclerosis 5(3):293–302
33. Leask RL, Butany J, Johnston KW, Ethier CR, Ojha M (2005) Human saphenous vein coronary artery bypass graft morphology, geometry and hemodynamics. Ann Biomed Eng 33(3):301–309
34. Lee SW, Antiga L, Steinman DA (2009) Correlations among indicators of disturbed flow at the normal carotid bifurcation. J Biomech Eng 131(6):061013. doi:10.1115/1.3127252
35. Lee SW, Smith DS, Loth F, Fischer PF, Bassiouny HS (2007) Importance of flow division on transition to turbulence within an arteriovenous graft. J Biomech 40(5):981–992
36. Lei M, Archie JP, Kleinstreuer C (1997) Computational design of a bypass graft that minimizes wall shear stress gradients in the region of the distal anastomosis. J Vasc Surg 25(4):637–646
37. Lei M, Kleinstreuer C, Archie JP (1996) Geometric design improvements for femoral graft-artery junctions mitigating restenosis. J Biomech 29(12):1605–1614
38. Leon C, Asif A (2007) Arteriovenous access and hand pain: the distal hypoperfusion ischemic syndrome. Clin J Am Soc Nephrol 2(1):175–183
39. Li L, Terry CM, Shiu YT, Cheung AK (2008) Neointimal hyperplasia associated with synthetic hemodialysis Grafts. Kidney Int 74(10):1247–1261
40. Longest PW, Kleinstreuer C (2000) Computational haemodynamics analysis and comparison study of arterio-venous grafts. J Med Eng Technol 24(3):102–110
41. Loth F, Fischer PF, Arsalan N, Bertram CD, Lee SE, Royston TJ, Shaalan WE, Bassiouny HS (2003) Transitional flow at the venous anastomosis of an arteriovenous graft: potential activation of the ERK1/2 mechanotransduction pathway. J Biomech 125:49–61
42. McVeigh GE, Bratteli CW, Morgan DJ et al (1999) Age-related abnormalities in arterial compliance identified by pressure pulse contour analysis: aging and arterial compliance. Hypertension 33(6):1392–1398
43. Meichelboeck W (2011) End stage renal disease (ESRD) epidemiology—Where are we going? J Vasc Access 12(2):137–181
44. Meyerson SL, Skelly CL, Curi MA, Shakur UM, Vosicky JE, Glagov S, Schwartz LB (2001) The effects of extremely low shear stress on cellular proliferation and neointimal thickening in the failing bypass graft. J Vasc Surg 34(1):90–97
45. Nagel T, Resnick N, Deway CF Jr et al (1999) Vascular endothelial cells respond to spatial gradients in fluid shear stress by enhanced activation of transcription factors. Arterioscler Thromb Vasc Biol 19:1825–1834

46. NKF, KDOQI (2006) Clinical practice guidelines and clinical practice recommendations for vascular access; 2006 updates (suppl 1). Am J Kidney Dis 48:S227–S364
47. O'Callaghan S, Walsh M, McGloughlin T (2006) Numerical modelling of Newtonian and non-Newtonian representation of blood in a distal end-to-side vascular bypass graft anastomosis. Med Eng Phys 28:70–74
48. Ojha M (1993) Spatial and temporal variations of wall shear stress within an end-to-side arterial anastomosis model. J Biomech 26(12):1377–1388
49. Ojha M (1994) Wall shear stress temporal gradient and anastomotic intimal hyperplasia. Circ Res 74:1227–1231
50. Polo JR, Ligero JM, Diaz-Cartelle J, Garcia-Pajares R, Cervera T, Reparaz L (2004) Randomized comparison of 6-mm straight grafts versus 6- to 8-mm tapered grafts for brachial-axillary dialysis access. J Vasc Surg 40:319–324
51. Rouleau L, Farcas M, Tardif JC, Mongrain R, Leask RL (2010) Endothelial Cell Morphologic Response to Asymmetric Stenosis Hemodynamics: effects of Spatial Wall Shear Stress Gradients. J Biomech Eng 132(8):081013. doi:10.1115/1.4001891
52. Roy-Chaudhury P, Kelly BS, Melhem M et al (2005) Vascular access in hemodialysis: issues, management, and emerging concepts. Cardiol Clin 23:249–273
53. Salam TA, Lumsden AB, Suggs WD, Ku DN (1996) Low shear stress promotes intimal hyperplasia thickening. J Vasc Invest 2:12–22
54. Shaik E, Hoffmann KA, Dietiker JF (2008) Numerical simulations of pulsatile non-Newtonian flow in an end-to-side anastomosis model. Simul Model Pract Theory 16:1123–1135
55. Sivanesan S, How TV, Black RA, Bakran A (1999) Flow patterns in the radiocephalic arteriovenous fistula: an in vitro study. J Biomech 32(9):915–925
56. Slack SM, Jennings LK, Turitto VT (1994) Platelet size distribution measurements as indicators of shear stress-induced platelet aggregation. Ann Biomed Eng 22(6):653–659
57. Steinman DA, Vinh B, Ethier CR et al (1993) A numerical simulation of flow in a two-dimensional end-to-side anastomosis model. J Biomech Eng 115(1):112–118
58. Sutera SP, Mehrjardi MH (1975) Deformation and fragmentation of human red blood cells in turbulent shear flow. Biophys J 15(1):1–10
59. Tardy Y, Resnick N, Nagel T et al (1997) Shear stress gradients remodel endothelial monolayers in vitro via a cell proliferation-migration-loss cycle. Arterioscler Thromb Vasc Biol 17(11): 3102–3106
60. Van Canneyt K, De Santis G, Eloot S, Segers P, Verdonck P (2011) Swirlgraft versus conventional straight graft as vascular access: a full CFD-analysis. Conference proceedings CMBE11 383–386
61. Van Canneyt K, Morbiducci U, Eloot S, De Santis G, Segers P, Verdonck P (2013) A computational exploration of helical arterio-venous graft designs. J Biomech 46(2):345–353
62. Van Canneyt K, Pourchez T, Eloot S et al (2010) Hemodynamic impact of anastomosis size and angle in side-to-end arteriovenous fistulae: a computer analysis. J Vasc Access 11(1):52–58
63. Van Tricht I, De Wachter D, Tordoir J, Verdonck P (2004) Hemodynamics in a compliant hydraulic in vitro model of straight versus tapered PTFE arteriovenous graft. J Surg Res 116:297–304
64. Van Tricht I, De Wachter D, Tordoir J, Verdonck P (2006) Comparison of the hemodynamics in 6 mm and 4–7 mm hemodialysis grafts by means of CFD. J Biomech 39:226–236
65. Van Tricht I, De Wachter D, Tordoir J, Verdonck P (2005) Hemodynamics and complications encountered with arteriovenous fistulas and grafts as vascular access for hemodialysis: a review. Ann Biomed Eng 33(9):1142–1157

Copyright of Medical & Biological Engineering & Computing is the property of Springer Science & Business Media B.V. and its content may not be copied or emailed to multiple sites or posted to a listserv without the copyright holder's express written permission. However, users may print, download, or email articles for individual use.